 doi:10.20944/preprints201805.0381.v1

Application of Kinetic Flux Vector Splitting Scheme for Solving Viscous Quantum Hydrodynamical Model of Semiconductor Devices

Ubaid Ahmed Nisar[a,*], Waqas Ashraf[b], Shamsul Qamar[c]

[a] *Department of Computer Science, Bahria University, Islamabad, Pakistan.*
[b] *Department of Applied Mathematics and Statistics, Institute of Space Technology, Islamabad, Pakistan.*
[c] *Department of Mathematics, COMSATS Institute of Information Technology, Islamabad, Pakistan.*

Abstract

In this article, one-dimensional viscous quantum hydrodynamical model of semiconductor devices is numerically investigated. The model treats the propagation of electrons in a semiconductor device as the flow of a charged compressible fluid. It plays an important role in predicting the behavior of electron flow in semiconductor devices. The nonlinear viscous quantum hydrodynamic models contain Euler-type equations for density and current, viscous and quantum correction terms, and a Poisson equation for electrostatic potential. Due to high nonlinearity of model equations, numerical solution techniques are applied to obtain their solutions.. The proposed numerical scheme is a splitting scheme based on the kinetic flux-vector splitting (KFVS) method for the hyperbolic step, and a semi-implicit Runge-Kutta method for the relaxation step. The KFVS method is based on the direct splitting of macroscopic flux functions of the system on the cell interfaces. The second order accuracy of the scheme is achieved by using MUSCL-type initial reconstruction and Runge-Kutta time stepping method. Several case studies are considered. For validation, the results of current scheme are compared with those obtained from the splitting scheme based on the NT central scheme. The effects of various parameters such as device length, viscosities, different doping and voltage are analyzed. The accuracy, efficiency and simplicity of the proposed KFVS scheme validates its generic applicability to the given model

*Corresponding author. Tel: +92-344-5520552
Email addresses: ubaid867@hotmail.com (Ubaid Ahmed Nisar)

Preprints (www.preprints.org) | NOT PEER-REVIEWED | Posted: 28 May 2018 doi:10.20944/preprints201805.0381.v1

equations.

1. Introduction

In simulation of the semiconductor devices, the quantum effect models becomes very important because of the very small sizes of the characteristic device $100nm$. Schrodinger or Wigner equations of microscopic nature model the quantum effects [1, 2]. In past few years, the development in the macroscopic quantum equations improved and used more widely in the simulation of the quantum devices [3]-[9], those have several advantages in describing the physics of such semiconductor devices. First, the Schrodinger or Wigner equation is computationally quite costly, whereas efficient and accurate numerical algorithms are available for fluid-type models. Second, it is quite easy to locate the corresponding boundary conditions because the bounded domains are used in the modeling of semiconductor devices. Since 1927, such phenomena holds as existence of fluid-dynamical formulation of the Schrodinger equation available in literature see [10].

To numerically simulate the viscous quantum hydrodynamic (VQHD) models specific semiconductor devices are used, such as the resonant tunnel diode (RTD), see [11, 12]. These models are much simpler and easier to solve as compared to the inviscid models, such as HD models. The two-dimensional VQHD model was first numerically investigated by Dreher. et.al [13, 14]. Later on, the exponential decay in time was also numerically studied for the one-dimensional VQHD by Gualdani. et.al [15]. Moreover, the global existence of weak solutions the viscous model were discussed, see [16, 17].

2. Viscous quantum hydrodynamic model

By separating the single-state Schrodinger equation into its real and complex parts, the density n and the current J satisfy the Madelung equations

$$\partial_t n + \frac{1}{q}\nabla \cdot J = 0, \tag{1}$$

$$\partial_t J + \frac{1}{q}\nabla \cdot \left(\frac{J \otimes J}{n}\right) - \frac{q^2}{m} n \nabla V - \frac{\hbar^2 q}{6m^2} n \nabla \left(\frac{\Delta \sqrt{n}}{\sqrt{n}}\right) = 0, \tag{2}$$

Preprints (www.preprints.org) | NOT PEER-REVIEWED | Posted: 28 May 2018 doi:10.20944/preprints201805.0381.v1

where, ∇ represents the space derivatives and $J \otimes J$ is the tensor having components $J_i J_k$ for $i, k = 1, 2, \cdots, d$, where d represents the number of dimensions. This model can also be expressed in the form of the pressureless Euler equations [18].

The quantum hydrodynamic models are completely free from the impurities of the semiconductor such as collisions of electrons. Practically speaking these studies of quantum theory are in initial stages (see, e.g., [19, 20, 21, 22]). With the help of Fokker-Planck-type collision operator suggested in [23, 24, 25], the Wigner equation can be re-written as

$$\partial_t w + \frac{\hbar}{m} k \nabla_x w + \frac{q}{\hbar} \Theta[V](w) = \frac{D_{pp}}{\hbar^2} \Delta_k w + \frac{1}{\tau_0} \nabla_k (kw) + \frac{D_{pq}}{\hbar} \nabla_x \cdot (\nabla_k w) + D_{qq} \Delta_x w, \quad (3)$$

with constants

$$D_{pp} = \frac{m k_b T_0}{\tau_0}, \quad D_{pq} = \frac{\Omega \hbar^2}{6\pi k_b T_0 \tau_0}, \quad D_{qq} = \frac{\hbar^2}{12 m k_b T_0 \tau_0},$$

where, Ω and τ_0 are the cut-off frequency and the momentum relaxation time of the reservoir oscillators. The terms D_{pp}, D_{pq} and D_{qq} are the constant, establish the phase-space diffusion matrix, and the term $\nabla_k(kw)/\tau_0$ is a friction term. For more detailed discussion, see [24, 26].

With the help of Wigner-Fokker-Planck Eq. (3), we can derive the moment equations [5] in closure form with $O(h^2)$ approximation of the quantum thermal equilibrium state. In result, we get the following equations (for derivation, see [26]):

$$\partial_t n + \frac{1}{q} \nabla \cdot J = D_{pp} \Delta n, \quad (4)$$

$$\partial_t J + \frac{1}{q} \nabla \cdot \left(\frac{J \otimes J}{n} \right) + \frac{q k_B T_0}{m} \left(1 + \frac{D_{pq}}{k_b T_0} \right) \Delta n$$
$$- \frac{q^2}{m} n \nabla V - \frac{\hbar^2 q}{6 m^2} n \nabla \left(\frac{\Delta \sqrt{n}}{\sqrt{n}} \right) = - \frac{J}{\tau_0} + D_{qq} \Delta J, \quad (5)$$

to be coupled to the Poisson equation

$$\varepsilon_s \Delta V = q(n - C), \quad (6)$$

with the permittivity ε_s, charge q and doping density profile C. The terms $D_{qq}\Delta J$ and $D_{pp}\Delta n$ are of second order treated as viscous terms.

Preprints (www.preprints.org) | NOT PEER-REVIEWED | Posted: 28 May 2018 doi:10.20944/preprints201805.0381.v1

2.1. Scaling of parameters

Let us scale the viscous quantum hydrodynamic equations (c.f. Eqs. (4)-(6)) by introducing the characteristic density $C^* = sup|C|$, current density $J^* = C^* t^* q k_B T_0 / Lm$ and voltage $V^* = k_B T_0 / q$. Here, t^* is defined by the relation $L^2 = (t^*)^2 k_B T_0 / m^2$. After introducing the dimensionless parameters

$$x = x/L, \quad t = t/t^*, \quad C = C/C^*, \quad n = n/C^*, \quad J = J/J^*, \quad V = V/V^*,$$

$$\tau = \frac{\tau_0}{t^*}, \quad \nu = \frac{t^*}{6\tau_0}\left(\frac{L_b}{L}\right)^2, \quad \epsilon^2 = \frac{2}{3}\left(\frac{L_b}{L}\right)^2, \quad \lambda^2 = \frac{\epsilon_s k_B T_0}{q^2 L^2 C^*}, \quad T = 1 + \frac{\Omega L_b \hbar}{\sqrt{1}8\pi k_B T_0 l},$$

where, $L_b = \hbar/\sqrt{2k_B m T_0}$ is a constant value named as de Broglie length. The viscous quantum hydrodynamic model after scaling is given by:

$$\partial_t n + \nabla \cdot J = \nu \Delta n, \tag{7}$$

$$\partial_t J + \nabla \cdot \left(\frac{J \otimes J}{n}\right) - n\nabla(V + V_{ext}) + T\nabla n - \frac{\epsilon^2}{2} n \nabla\left(\frac{\Delta\sqrt{n}}{\sqrt{n}}\right)_x = -\frac{J}{\tau} + \nu \Delta J, \tag{8}$$

$$\lambda^2 \Delta V = (n - C). \tag{9}$$

where, $\nu > 0$ (viscosity-constant). We have introduced the term external potential $V_{ext}(x)$ to the left hand side of Eq. (8) which models heterogeneous semiconductor materials. For considering doping in m^3, we have assumed $C^* = 10^{24} m^3$. The scaled parameters calculated as $\epsilon^2 = 3.893 \times 10^{-3}$, $\nu = 9.935 \times 10^{-4}$, $T = 1.00585$ and $\lambda^2 = 3.032 \times 10^{-4}$.

2.2. Compact form of the model

In this section, we rewrite the 1D viscus quantum hydrodynamic model in a more compact form for application of the numerical schemes. In one space dimension, the viscous quantum hydrodynamic model (c.f. Eqs. (7) and (8)) reduces to:

$$\mathbf{U}_t + \mathbf{A}(U)_x = (\mathbf{B}(U, U_x))_x + \mathbf{S}(U), \tag{10}$$

Preprints (www.preprints.org) | NOT PEER-REVIEWED | Posted: 28 May 2018 doi:10.20944/preprints201805.0381.v1

together with the Poisson equation

$$\lambda^2 V_{xx} = n - C(x). \tag{11}$$

The vector quantities in Eq, (10) are expressed as

$$\mathbf{U} = \begin{bmatrix} n \\ J \end{bmatrix}, \qquad \mathbf{A}(U) = \begin{bmatrix} J \\ \frac{J^2}{n} + Tn \end{bmatrix},$$

$$\mathbf{B}(U, U_x) = \begin{bmatrix} \nu n_x \\ \nu J_x \end{bmatrix}, \qquad \mathbf{S}(U) = \begin{bmatrix} 0 \\ -J + n(\tilde{V} + Q)_x \end{bmatrix},$$

where, $\tilde{V} = V + V_{ext}$ and $Q = \frac{\epsilon^2 \partial_{xx}\sqrt{n}}{2\sqrt{n}}$.
Assuming L as the typical device length, the initial conditions are given below:

$$n(x, 0) = C(x), \quad u(x, 0) = 0, \tag{12}$$

and boundary conditions are:

$$n_x(0, t) = n_x(L, t) = 0, \quad u_x(0, t) = u_x(L, t) = 0. \tag{13}$$

To respect the conservation of electrons, fixed-type boundary conditions are considered for the density (n), i.e. $n(0, t) = C(0)$ and $n(L, t) = C(L)$. The potential V in the Poisson equation, with an applied voltage V_b, has the boundary conditions of the form

$$V(0) = 0, \quad V(L) = V_b. \tag{14}$$

The left hand side of Eq. (10) represents a quasi-linear hyperbolic operator, whereas, the diffusive terms give contribution in the right hand side.

3. Numerical Technique

In this section, numerical method ise derived to solve the one-dimensional viscous quantum hydrodynamic model for semiconductor devices. A one-dimensional KFVS scheme is proposed to approximate the model equations.

Preprints (www.preprints.org) | NOT PEER-REVIEWED | Posted: 28 May 2018 doi:10.20944/preprints201805.0381.v1

In Eq. (10) left hand side contains quasilinear hyperbolic operator, whereas, right hand side consists of relaxation and diffusion terms. The following decomposition can be used in splitting scheme. Considering the form of the system to be

$$\frac{\partial \mathbf{U}_1}{\partial t} + \frac{\partial \mathbf{A}(\mathbf{U}_1)}{\partial x} = \mathbf{g}. \tag{15}$$

Then, a numerical approximation $\tilde{\mathbf{U}}$ of the solution can be achieved by solving the two consecutive steps for each time step. In the first convection step, we have to solve the homogeneous system of equations of the form

$$\frac{\partial \mathbf{U}_1}{\partial t} + \frac{\partial \mathbf{A}(\mathbf{U}_1)}{\partial x} = \mathbf{0}, \quad \mathbf{U}_1 = \tilde{\mathbf{U}}(t). \tag{16}$$

The second one is the relaxation step which expressed as

$$\frac{\partial \tilde{\mathbf{U}}}{\partial t} = \mathbf{g}, \quad \tilde{\mathbf{U}}(t) = \mathbf{U}_1(t + \Delta t). \tag{17}$$

This is a simple splitting scheme which is easily understandable. However, the scheme has only first-order accuracy in time coordinate. In the following, we will present a more accurate scheme for the discretization of ordinary differential equations (ODEs) in the relaxation step.

3.1. One-dimensional KFVS method

In this sub-section, we implement KFVS scheme on the system of Eqs. (16) to numerically approximate the model equations. The formulation of the KFVS solver for the numerical discretization of the given model equations is carried out on the basis of the evaluation of macroscopic flux-vector $\mathbf{A}(\mathbf{U})$ through each boundary of the mesh cell. Flux function can be determined by the motion of particle in the x-direction. The other quantities, such as densities, velocity, pressure and energy have to be treated like passive scalars moving with the particles velocity. Generally, around the average velocity the particles are distributed randomly.

In statistical mechanics, across coordinate directions the local Maxwellian distribution function f_M explains the motion of moving particles [27]

$$f_M(t, n, v_n) = n\left(\frac{\lambda}{\pi}\right)^{\frac{1}{2}} \exp[-\lambda(u_{\hat{n}} - v_{\hat{n}})^2], \quad \lambda = \frac{m^*}{2k_B T_0}, \tag{18}$$

Preprints (www.preprints.org) | NOT PEER-REVIEWED | Posted: 28 May 2018 doi:10.20944/preprints201805.0381.v1

where n, m^*, k_B and T_0 denote density, effective electron mass, Boltzmann constant and lattice temperature, respectively. The movement of particles contributes in transporting of flow quantity. Thus, in one space dimension, the distribution function f_M in Eq. (18) is used to divided particles into two main groups. The first group of particles have the positive velocity ($u_n > 0$) in the right direction and the second group of particles have the negative velocity ($u_n < 0$) in the left direction. Let us define the following zeroth and first order moments which are sufficient for splitting the fluxes across cell interfaces:

$$\langle v^0 \rangle_{\hat{n}} = 1 = \int_{-\infty}^{\infty} \left(\frac{\lambda}{\pi}\right)^{\frac{1}{2}} e^{-\lambda(u_{\hat{n}} - v_{\hat{n}})^2} dv_{\hat{n}}, \tag{19}$$

$$\langle v^1 \rangle_{\hat{n}} = u_{\hat{n}} = \int_{-\infty}^{\infty} \left(\frac{\lambda}{\pi}\right)^{\frac{1}{2}} v_{\hat{n}} e^{-\lambda(u_{\hat{n}} - v_{\hat{n}})^2} dv_{\hat{n}}. \tag{20}$$

The zeroth order moment in Eq. (19) and first order moment in Eq. (20) both are used for splitting scalars and vectors, respectively. In more simplified notation, let us define

$$\langle v^0 \rangle_{+\hat{n}} = \int_{0}^{\infty} \left(\frac{\lambda}{\pi}\right)^{\frac{1}{2}} e^{-\lambda(u_{\hat{n}} - v_{\hat{n}})^2} dv_{\hat{n}} = \frac{1}{2}\mathrm{erfc}(-\sqrt{\lambda}u_{\hat{n}}), \tag{21}$$

$$\langle v^0 \rangle_{-\hat{n}} = \int_{-\infty}^{0} \left(\frac{\lambda}{\pi}\right)^{\frac{1}{2}} e^{-\lambda(u_{\hat{n}} - v_{\hat{n}})^2} dv_{\hat{n}} = \frac{1}{2}\mathrm{erfc}(\sqrt{\lambda}u_{\hat{n}}), \tag{22}$$

and

$$\langle v^1 \rangle_{+\hat{n}} = \int_{0}^{\infty} \left(\frac{\lambda}{\pi}\right)^{\frac{1}{2}} v_{\hat{n}} e^{-\lambda(u_{\hat{n}} - v_{\hat{n}})^2} dv_{\hat{n}} = u_{\hat{n}} \langle v^0 \rangle_{+\hat{n}} + \frac{1}{2}\frac{e^{-\lambda u_{\hat{n}}^2}}{\sqrt{\pi\lambda}}, \tag{23}$$

$$\langle v^1 \rangle_{-\hat{n}} = \int_{-\infty}^{0} \left(\frac{\lambda}{\pi}\right)^{\frac{1}{2}} v_{\hat{n}} e^{-\lambda(u_{\hat{n}} - v_{\hat{n}})^2} dv_{\hat{n}} = u_{\hat{n}} \langle v^0 \rangle_{-\hat{n}} - \frac{1}{2}\frac{e^{-\lambda u_{\hat{n}}^2}}{\sqrt{\pi\lambda}}, \tag{24}$$

In the above equations, the motion of the particles in the right direction is represented by the positive sign and the motion of the particles in the left direction is represented by the negative sign. Furthermore, the error function appearing in Eqs. (21) and (22) is expressed as

$$\mathrm{erfc}(z) = \frac{2}{\sqrt{\pi}} \int_{z}^{\infty} e^{-t^2} dt. \tag{25}$$

Now the Eq. (16) can be solved by KFVS scheme by considering the above explained technique. Before implementing the finite volume scheme, we sub-divide the domain into

Preprints (www.preprints.org) | NOT PEER-REVIEWED | Posted: 28 May 2018 doi:10.20944/preprints201805.0381.v1

N sub domains. We define the cell I_i by interval $[x_{i-\frac{1}{2}}, x_{i+\frac{1}{2}}]$ for $i = 1, \cdots, N$. Hence, $\Delta x = x_{i+\frac{1}{2}} - x_{i-\frac{1}{2}}$ indicates the uniform cells width, $x_{i\pm\frac{1}{2}} = x_i \pm \Delta x/2$ represent the cells faces and $x_i = i\Delta x$ denotes cells center. We start with a initial cell averaged data U_i^n at time step t^n and compute updated cell average solution U_i^{n+1} on the similar cells for the next time step t^{n+1}.

With the help of above procedure, the flux function in Eq. (16), splits as

$$\mathbf{A}(\mathbf{U}) = \mathbf{A}^+ + \mathbf{A}^-, \tag{26}$$

where

$$\mathbf{A}^\pm = \langle v^1 \rangle_{\pm x} + \langle v^0 \rangle_{\pm x}\,. \tag{27}$$

Here, the right interface flux vector of the cell I_i is defined as

$$A_{i\pm\frac{1}{2}} = A_i^+ + A_{i+1}^-\,. \tag{28}$$

Similarly, the left interface flux vector of the cell I_i can be defined. The integration of Eq. (16) on the cell $[x_{i-1/2}, x_{i+1/2}]$ gives the semi-discrete kinetic upwind scheme as follows

$$\frac{dU_i}{dt} = -\frac{A_{i+\frac{1}{2}} - A_{i-\frac{1}{2}}}{\Delta x}\,. \tag{29}$$

The cell averaged values U_i are defined as

$$U_i := U_i(t) = \frac{1}{\Delta x}\int_{x_{i-\frac{1}{2}}}^{x_{i+\frac{1}{2}}} U(t,x)dx. \tag{30}$$

The above scheme has first order accuracy. However, high order accuracy can be achieved by applying the initial reconstruction procedure to interpolate the cell averaged variables U_i. In this article, MUSCL-type initial reconstruction strategy is used. Let us define U_i as the piecewise constant solution and U^x as the slope vector (differences) in the x-direction. The boundary extrapolated values are given as

$$U_i^L = U_i - \frac{1}{2}U_i^x, \quad U_i^R = U_i - \frac{1}{2}U_i^x\,. \tag{31}$$

Preprints (www.preprints.org) | NOT PEER-REVIEWED | Posted: 28 May 2018 doi:10.20944/preprints201805.0381.v1

A possible computation of these slopes is given by a family of discrete derivatives parameterized with $1 \leq \theta \leq 2$, for example

$$U_i^x = MM\left\{\theta\Delta U_{i+\frac{1}{2}}, \frac{\theta}{2}\left(\Delta U_{i+\frac{1}{2}} + \Delta U_{i-\frac{1}{2}}\right), \theta\Delta U_{i-\frac{1}{2}}\right\}, \tag{32}$$

where, the parameter $\theta \in [1,\, 2]$,

$$\Delta U_{i+\frac{1}{2}} = U_{i+1} - U_i\,. \tag{33}$$

where, Δ denotes the central differencing. Here, MM denotes the min-mod non-linear limiter

$$MM\{x_1, x_2, ...\} = \begin{cases} \min\limits_i\{x_i\} & \text{if} \quad x_i > 0\,\forall i, \\ \max\limits_i\{x_i\} & \text{if} \;\; x_i < 0\,\forall i, \\ 0 & \text{elsewhere.} \end{cases} \tag{34}$$

Considering the above mentioned reconstruction procedure, a semi-discrete high resolution kinetic solver follows as

$$\frac{dU_i}{dt} = -\frac{A_{i+\frac{1}{2}}(U_{i+1}^L, U_i^R) - A_{i-\frac{1}{2}}(U_i^L, U_{i-1}^R)}{\Delta x}\,. \tag{35}$$

To maintain the accuracy of order 2 in time, a TVD RK-scheme of order 2 is applied to solve Eq. (35). Let us denote the right side of Eq. (35) as $L(U)$ and update U through the following two stages [28]:

$$U^{(1)} = U^n + \Delta t L(U^n)\,, \tag{36}$$

$$U^{n+1} = \frac{1}{2}\left(U^n + U^{(1)} + \Delta t\, L(U^{(1)})\right)\,. \tag{37}$$

Here, u^n being the solution at previous time step and u^{n+1} denotes the updated value at next time step. Moreover, Δt denotes the time step.

3.2. Central finite different scheme

In this sub-section, we briefly explain the Nessyahu and Tadmor's (NT) central scheme [29]. The scheme is a predictor and corrector type method. In the first step, the cell-averaged piecewise linear reconstructions is used to predict the mid-point values. While,

Preprints (www.preprints.org) | NOT PEER-REVIEWED | Posted: 28 May 2018 doi:10.20944/preprints201805.0381.v1

in the second step, mid-point and staggered averaging values from the first step, have to be used to get the updated cell averaged solution. In result, the scheme is expressed as

$$\text{predictor:} \quad U_i^{n+\frac{1}{2}} = U_i^n - \frac{\zeta}{2} A^n(U_i^n)\,, \tag{38}$$

$$\text{corrector:} \quad U_{i+\frac{1}{2}}^{n+\frac{1}{2}} = \frac{1}{2}(U_i^n + U_{i+1}^n) + \frac{1}{8}(U_i^n - U_{i+1}^n) - \zeta(A_{i+1}^{n+\frac{1}{2}} - A_i^{n+\frac{1}{2}}) \tag{39}$$

$$+ \zeta(B_{i+1}^{n+\frac{1}{2}} - B_i^{n+\frac{1}{2}}) + \zeta(S_{i+1}^{n+\frac{1}{2}} - S_i^{n+\frac{1}{2}})\,,$$

where, $\zeta = \frac{\Delta t}{\Delta x}$. Furthermore, $\frac{1}{\Delta x} A^x(U_i)$ stands for an approximate numerical derivatives of the flux $A^x(x_i, t)$ which will be calculated as

$$A_i^x = MM\Big\{\theta \Delta A_{i+\frac{1}{2}}\,,\, \frac{\theta}{2}(\Delta A_{i+\frac{1}{2}} + \Delta A_{i+\frac{1}{2}})\,, \theta \Delta A_{i-\frac{1}{2}}\Big\}. \tag{40}$$

This completes the derivation of NT scheme.

3.3. Relaxation step

For the relaxation step a semi-implicit Runge Kutta (RK) scheme is proposed which avoids the stability restriction on the time step Δt. Let, (U^n, E^n) are known at time t^n,, to evaluate at next time step, the procedure given in [30] follow as:

$$U_1 = U^n - R(U_1, E^n, \Delta t), \qquad U_2 = \frac{3}{2}U^n - \frac{1}{2}U_1, \tag{41}$$

$$U_3 = U_2 - R(U_3, E^n, \Delta t), \qquad U_4 = \mathcal{C}_{\Delta t} U_3, \tag{42}$$

$$E^{n+1} = \mathcal{P}(U_4), \qquad U^{n+1} = U_4 - R(U^{n+1}, E^{n+1}, \frac{\Delta t}{2}), \tag{43}$$

where R represents the numerical operator corresponding to relaxation step, $\mathcal{C}_{\Delta t}$ represents the numerical convection operator corresponding to two steps of KFVS scheme, and $\mathcal{P}(U)$ denotes the solution of Poisson's equation. Moreover, the discretization of Poisson Eq. (11) can be done with the central difference scheme

$$\varepsilon_s(V_{i+1} - 2V_i + V_{i-1}) = q(n_i - C)(\Delta x)^2, \quad i = 1, \cdots, N. \tag{44}$$

The above tridaigonal system is solved to obtain electric potential V.

Preprints (www.preprints.org) | NOT PEER-REVIEWED | Posted: 28 May 2018 doi:10.20944/preprints201805.0381.v1

4. Numerical Case Studies

In this section, three test problems are considered to validate the accuracy and performance of the proposed scheme. For comparison and validation of results, the NT-central scheme is also applied to the same model equations. Physical parameters used in the numerical test problems are listed in Table. 1. For calculating doping in m^3, it is assumed that $C^* = 10^{24} m^3$. The values of scaled parameters are given as $\epsilon^2 = 3.893 \times 10^{-3}$, $\nu = 9.935 \times 10^{-4}$, $T = 1.00585$ and $\lambda^2 = 3.032 \times 10^{-4}$.

Case 1: Different Doping: In this test problem, a semiconductor of length $L = 125\,nm$ is considered. The device is divided into three regions namely, source, channel and drain regions. The source and drain regions are of lengths $[0\,nm,\ 50\,nm]$ and $[75\,nm,\ 125\,nm]$ respectively, and the channel region is of length $[50\,nm,\ 75\,nm]$. The doping density profile is given as

$$C(x) = \Big[1.0 + 0.4599\Big(\tanh(10x - 750) - \tanh(10x - 500)\Big)\Big] \times 10^{24}, \quad x \in [0\,nm, 125\,nm]\,, \tag{45}$$

and V_{ext} is defined as

$$V_{\text{ext}} = \begin{cases} 0.209\,V, & x \in (50\,nm, 75\,nm), \\ 0,, & \text{elsewhere.} \end{cases} \tag{46}$$

We consider a GaAs diode of length $L = 125\,nm$ kept at $T_0 = 77\,K$. The applied voltage is $V_b = 1.5\,V$. The numerical results for physical variables on 200 grid points are displayed in Figure 1. From the Figure 1, the steady state behavior of electron density can be observed in source and drain regions. With application of external potential V_{ext} and applied voltage V_b, perturbation in channel region can be seen. Similar, patterns can also be seen in current, velocity and potential profiles. Results obtained from KFVS are compared with the NT central scheme [29]. This was concluded that KFVS scheme shows better results in capturing peaks and in resolving oscillations/discontinuities.

Preprints (www.preprints.org) | NOT PEER-REVIEWED | Posted: 28 May 2018 doi:10.20944/preprints201805.0381.v1

Case 2: Convergence study of schemes: The viscous quantum hydrodynamic models has also widely been used in study of the GaAs ballistic $n^+ - n - n^+$ devices. Here, n^+ is the source region equipped with the heavy doping, n is the channel region equipped with the light doping, and at the end n^+ is the drain region.

In this test problem, we consider a GaAs diode of length $L = 0.6\,\mu m$ with a source region of $0.1\,\mu m$, channel length of $0.4\,\mu m$, and drain region of $0.1\,\mu m$, see Figure 2. The applied voltage is $V_b = 0.3\,V$ and $T_0 = 77\,K$. The doping density profile is

$$C(x) = \begin{cases} 2 \times 10^{21} m^{-3}, & x \in (0.1\mu m, 0.5\mu m), \\ 5 \times 10^{23} m^{-3}, & \text{otherwise}, \end{cases} \tag{47}$$

and V_{ext} is given as

$$V_{\text{ext}} = \begin{cases} -0.209V, & x \in (0.1\mu m, 0.2\mu m) \cup (0.3\mu m, 0.4\mu m), \\ 0, & \text{otherwise}. \end{cases} \tag{48}$$

The numerical results for physical variables on 200 grid points are displayed in Figure 3. It can be seen in Figure 3 that KFVS scheme shows better results in resolving the sharp discontinuities and peaks. Similar results were also obtained by other researchers in the literature, see e.g. [31] and references therein.

To quantitatively analyze the accuracy of proposed scheme, the L^1-errors at different grid points are calculated and given in Table 2. The reference solution was obtained at 1600 mesh points. It can be concluded that KFVS scheme produces less errors in the solutions. Moreover, Figure 4 shows the plots of L^1-errors which justify the results of Table. 2.

Case 3: Different external potential V_{ext}: Again in this test problem, we consider a GaAs diode of length $L = 0.6\,\mu m$. The applied voltage is $V_b = 0.8\,V$ and $T_0 = 77\,K$. The doping density profile is similar as in previous case. We have tested the effects of different V_{ext} on current density solution. The solutions for the different values of V_{ext} are displayed in Figure 5. In the top left figure the $V_{\text{ext}} = -2.09 \times 10^{-1} V$, $x \in (0.1\mu m, 0.4\mu m)$, in the top right figure $V_{\text{ext}} = -2.09 \times 10^{-2} V$, $x \in (0.1\mu m, 0.4\mu m)$, in the bottom left

Preprints (www.preprints.org) | NOT PEER-REVIEWED | Posted: 28 May 2018 doi:10.20944/preprints201805.0381.v1

figure $V_{\text{ext}} = -2.09 \times 10^{-3}V$, $x \in (0.1\mu m, 0.4\mu m)$ and in last bottom right figure $V_{\text{ext}} = -2.09 \times 10^{-4}V$, $x \in (0.1\mu m, 0.4\mu m)$. It can be seen from the Figure 5, that on decreasing the external potential the flow of the current in the device increases. Such results were also reported in [12] and references therein.

Preprints (www.preprints.org) | NOT PEER-REVIEWED | Posted: 28 May 2018 doi:10.20944/preprints201805.0381.v1

Case 4: The effect of different viscosities: In this test problem the effects of physical parameters like viscosity is analyzed. We re-simulated the second test problem for different viscosities constant, such as $\nu = \nu_0/\gamma$ for $\nu_0 = 4.267 \times 10^{-4}$, for $\gamma = 1, 2, 4, 8$. The results of particle densities for various viscosities obtained from KFVS scheme are displayed in Figures 6. The smooth transition can be shown for a quite large viscosities. It is more obvious to say that the particles travel from left to right around the junction at $x = 1$ enter the supersonic region. Thus, the solution of viscous and inviscid models are similar to each others for small viscosity $\nu = \nu_0/8 \approx 5.0 \times 10^{-5}$, for reference see [12].
Similarly, the results of current density for various viscosities obtained from KFVS scheme are displayed in Figures 7. Analogously, in case of the current density J, it can be concluded that the solution of viscous and inviscid models coincides for small viscosity. As the current density J varies in present model and the term $J - \partial_x n$ representing the effective current is constant. Hence, we expect the constant current of the inviscid model and the variable J should coincides. Moreover, peaks are sharper for small viscosity and diffuse out on increasing the viscosity factor. The figures show that the proposed numerical scheme has well captured all profiles in the given viscosity range.

5. Conclusions

A second order accurate splitting scheme based on the KFVS method was presented to solve the one dimensional viscous quantum hydrodynamical model describing charge transport in semiconductor devices. The nonlinear transport processes, high gradients and stiff relaxation parameters in the model were the main sources of instabilities for a numerical scheme. For comparison and validation, a splitting scheme based on the NT central scheme was also applied to the same model. It was found that the suggested KFVS method has capability to capture narrow peaks and steep gradients in the solution profiles. Further, the solutions of proposed scheme were free of oscillations. This was demonstrated by considering the case studies of several one-dimensional $n^+ - n - n^+$ diodes. Moreover, the numerical solution obtained with different viscosities, mobilities and voltages further validated the robustness and efficiency of the current method.

 doi:10.20944/preprints201805.0381.v1

References

[1] A. Jungel, (2001) Quasi-Hydrodynamic Semiconductor Equations, Progress in Nonlinear Differential Equations, Birkhauser Basel.

[2] P.A. Markowich, C.A. Ringhofer, C. Schmeiser, (1990) Semiconductor Equations, Springer, Berlin.

[3] Ancona, M. G. and Iafrate, G. I., (1989) Quantum correction to the equation of state of an electron gas in a semiconductor. Phys. Rev. B., 39: 9536-9540.

[4] Degond, P. and Ringhofer, C., (2003) Quantum moment hydrodynamics and the entropy principle. J. Statist. Phys. 112: 587-628.

[5] Gardner, C. L., (1994) The quantum hydrodynamic model for semiconductor devices. SIAM J. Appl. Math. 54: 409-427.

[6] Grubin, H. L. and Kreskovsky, J. P. (1989) Quantum moment balance equations and resonant tunneling structures. Solid-State Electr. 32: 1071-1075.

[7] Jungel, A. and Pinnau, R. (2001) A positivity preserving numerical scheme for a nonlinear fourth-order parabolic equation. SIAM J. Num. Anal. 39: 385-406.

[8] Wettstein, A. (2000) Quantum effects in MOS devices. Vol 94: Series in Microelectronics, Hartung-Gorre, Konstanz.

[9] Zhou, J. and Ferry, D. K. (1992) Simulation of ultra-small GaAs MESFET using quantum moment equations. IEEE Trans. Electr. Devices 39: 473-478.

[10] Madelung, E. (1927) Quantentheorie in hydrodynamischer Form. Z. Physik. 40: 322-326.

[11] Jungel, A., Milisic, J. (2007). Physical and numerical viscosity for quantum hydrodynamics. *Comm. Math. Phys.* 5, 447-471.

[12] Jungel, A., Tang, S. (2006). Numerical approximation of the viscous quantum hydrodynamic model for semiconductors. *Appl. Numer. Math.* 1, 19-46.

[13] Chen, L., Dreher, M. (2007). The viscous model of quantum hydrodynamics in several dimensions. *Math. Mod. Meth. Appl. Sci.* 17, 1065-1093.

[14] Dreher, M. (2008). The transient equations of viscous quantum hydrodynamics. Math. Mod. Meth. Appl. Sci. 31, 391-414.

[15] Gualdani, M., Jungel, A., Toscani, G. (2003). Exponential decay in time of solutions of the viscous quantum hydrodynamic equations. *J. Appl. Math.* 16, 1273-1278.

[16] Gamba, I. M., Jungel, A., Vasseur, A. (2009). Global existence of solutions to one-dimensional viscous quantum hydrodynamic equations. *J. Diff. Eq.* 247, 3117-3135.

[17] Jungel, A. (2009). Global weak solutions to compressible Navier-Stokes equations for quantum fluids. Preprint.

[18] Gasser, I., Markowich, P. M., Schmidt, D., Unterreiter, A. (1995) Macroscopic theory of charged quantum fluids. *P. Marcati. (ed.)*. Mathematical Problems in Semiconductor Physics. 42-75.

[19] Argyres, P. (1992). Quantum kinetic equations for electrons in high electric and phonon fields. *Phys. Lett. A*. 171, 373-379.

[20] Buot, F., Jensen, K. (1990). Lattice WeylWigner formulation of exact many-body quantum-transport theory and applications to novel solid-state quantum-based devices. *Phys. Rev. B*. 42, 9429-9457.

[21] Eu, B. C., Mao, K. (1994). Quantum kinetic theory of irreversible thermodynamics: Low-density gases. *Phys. Rev. E*. 50, 4380-4398.

[22] Frommlet, F., Markowich, P., Ringhofer, C. (1999). A Wigner function approach to phonon scattering. *VLSI Design*. 9, 339-350.

[23] Caldeira, A., Leggett, A. (1983). Path integral approach to quantum Brownian motion. *Phys. A*. 121, 587-616.

[24] Arnold, A., Lopez, J. L., Markowich, P. M., Soler, J. (2000) An analysis of quantum Fokker-Planck models: a Wigner function approach. Preprint, TU Berlin, Germany.

[25] Castella, F., Erdos, L., Frommlet, F., Markowich, P. (2000). Fokker-Planck equations as scaling limits of reversible quantum systems. *J. Statist. Phys*. 100, 543-601.

[26] Gualdani., M. P., Ansgar., J. (2004). Analysis of the viscous quantum hydrodynamic equations for semiconductors. *Eur. J. Appl. Math*. 15, 577-595.

[27] Xu, K. (2002). A well-balanced gas-kinetic scheme for the shallow-water equations with source terms. *J. Comput. Phys*. 178, 533-562.

[28] Tang, T., Xu, K. (2000). A high-Order gas-kinetic method for multidimensional ideal magnetohydrodynamics. *J. Comput. Phys.*. 165, 69-88.

[29] Nessyahu, H., Tadmor, E. (1990). Non-oscillatory central differencing for perbolic conservation laws. *J. Comput. Phys*. 2, 408-463.

[30] Carpenter, M., Kennedy, C. (1994). Fourth-order 2N-storage Runge-Kutta schemes, NASA TM 109112, NASA Langley Research Center.

[31] Ashraf, W., Qamar, S. (2013). Application of central schemes for solving radiation hydrodynamical models. *Comp. Phy. Com*. 184, 1349-1363.

Preprints (www.preprints.org) | NOT PEER-REVIEWED | Posted: 28 May 2018 doi:10.20944/preprints201805.0381.v1

Table 1: Physical parameters.

Parameter	Physical meaning	Numerical values
m^*	electron mass	$2.37^{-29}\,kg$
μ_n	low-field mobility	$10^{-1}\,m^2V_s^{-1}$
q	elementary charge	$1.6\times10^{-19}\,C$
ε_s	semiconductor permittivity	$1.04\times10^{-10}\,Fm^{-1}$
n_i	intrinsic electron concentration	$1.4\times10^{16}\,m^3$
k_B	Boltzman constant	$1.38\times10^{-23}\,JK^{-1}$
v_s	saturation velocity	$1.03\times10^{5}\,ms^{-1}$
T_0	lattice temperature	$300\,K$

Table 2: Comparison of L^1-errors and CPU time.

Methods	N=100		N=200		N=400		N=800		CPU(s)
	n	J	n	J	n	J	n	J	N=200
KFVS	0.91	0.80	0.61	0.56	0.42	0.45	0.19	0.13	0.22
Central	0.99	0.92	0.72	0.69	0.52	0.49	0.25	0.22	0.31

Preprints (www.preprints.org) | NOT PEER-REVIEWED | Posted: 28 May 2018 doi:10.20944/preprints201805.0381.v1

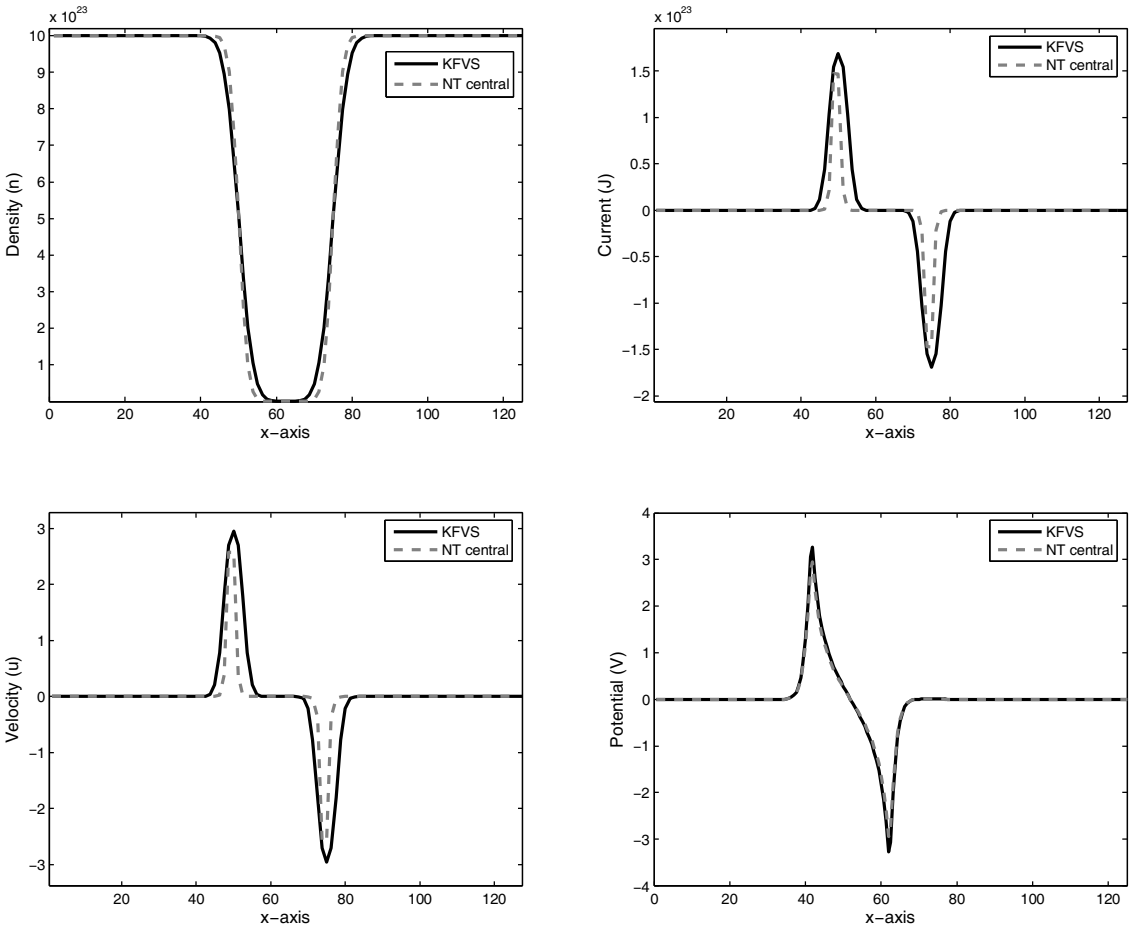

Figure 1: Case 1: Comparative study of the numerical schemes.

Preprints (www.preprints.org) | NOT PEER-REVIEWED | Posted: 28 May 2018 doi:10.20944/preprints201805.0381.v1

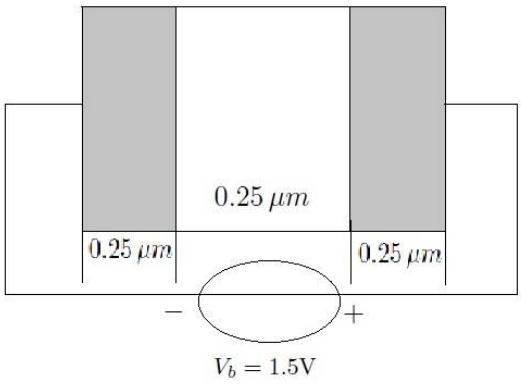

Figure 2: $n^+ - n - n^+$ Diode with length $0.75\mu m$ and $V_b = 1.5V$.

Preprints (www.preprints.org) | NOT PEER-REVIEWED | Posted: 28 May 2018 doi:10.20944/preprints201805.0381.v1

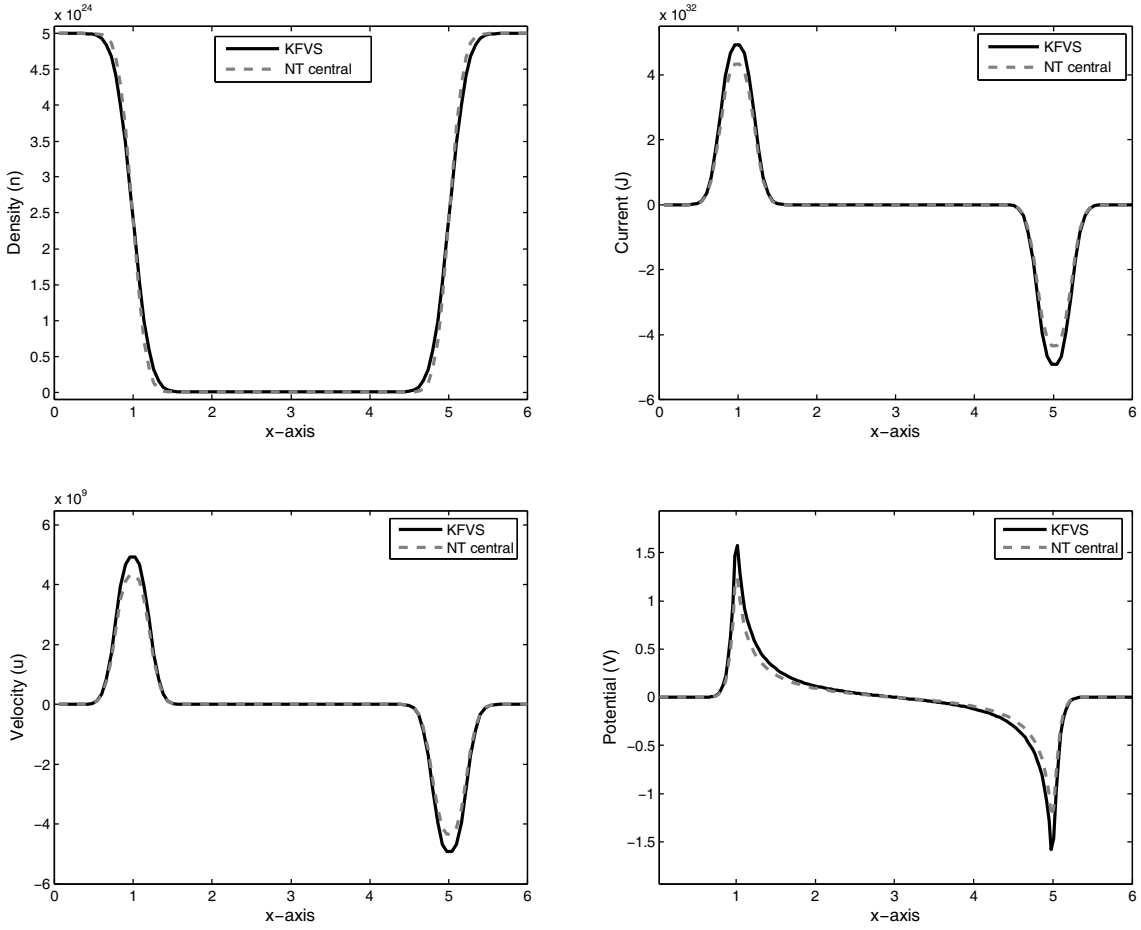

Figure 3: Case 2: Comparison of schemes on 200 grid points.

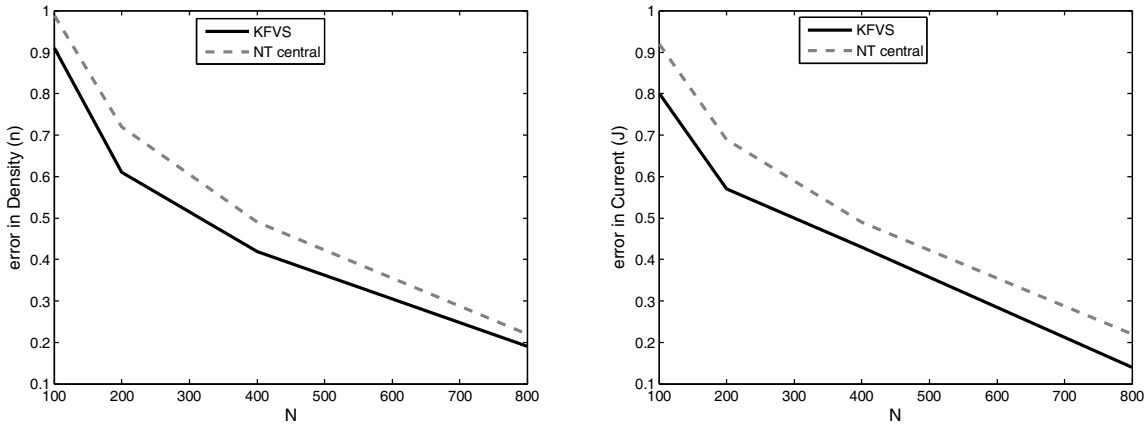

Figure 4: Errors at different grid points.

Preprints (www.preprints.org) | NOT PEER-REVIEWED | Posted: 28 May 2018 doi:10.20944/preprints201805.0381.v1

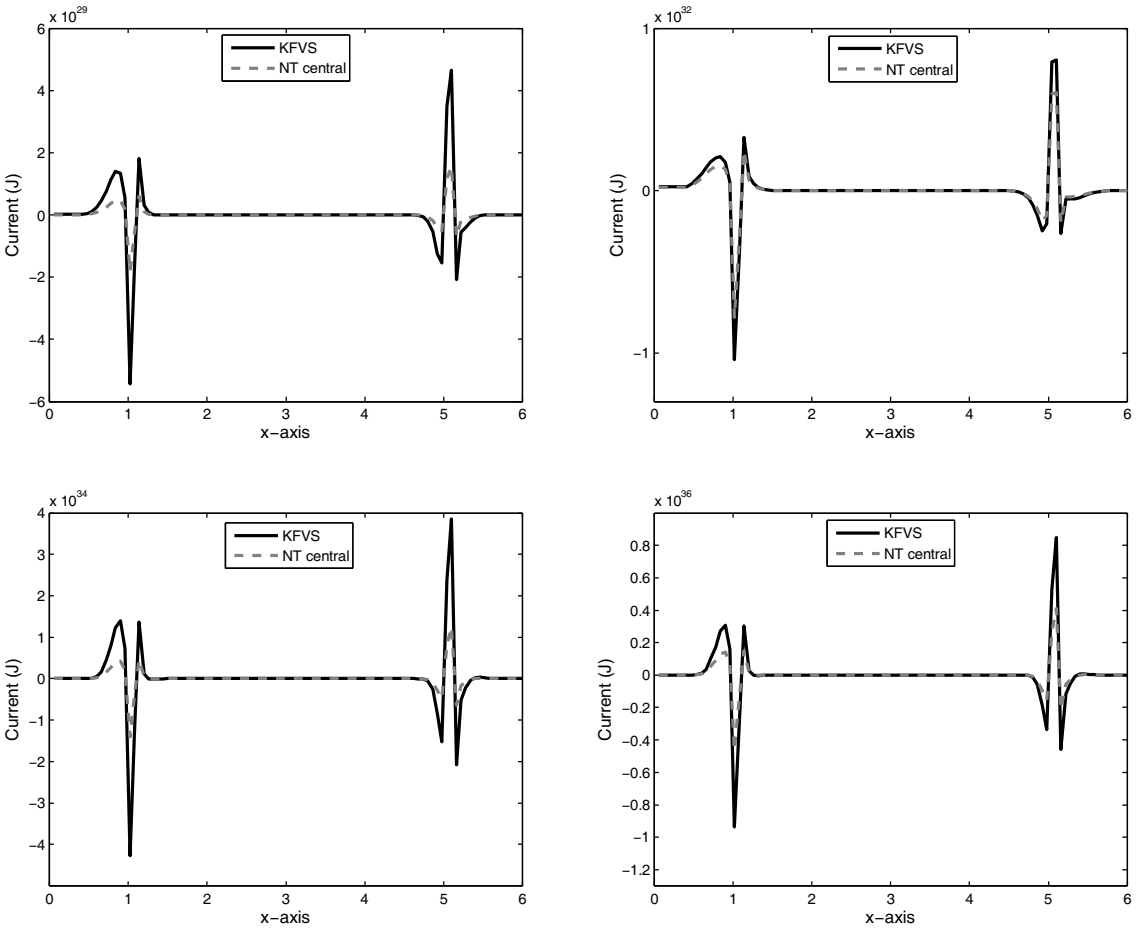

Figure 5: Case 3: Different external potential V_{ext}.

Preprints (www.preprints.org) | NOT PEER-REVIEWED | Posted: 28 May 2018 doi:10.20944/preprints201805.0381.v1

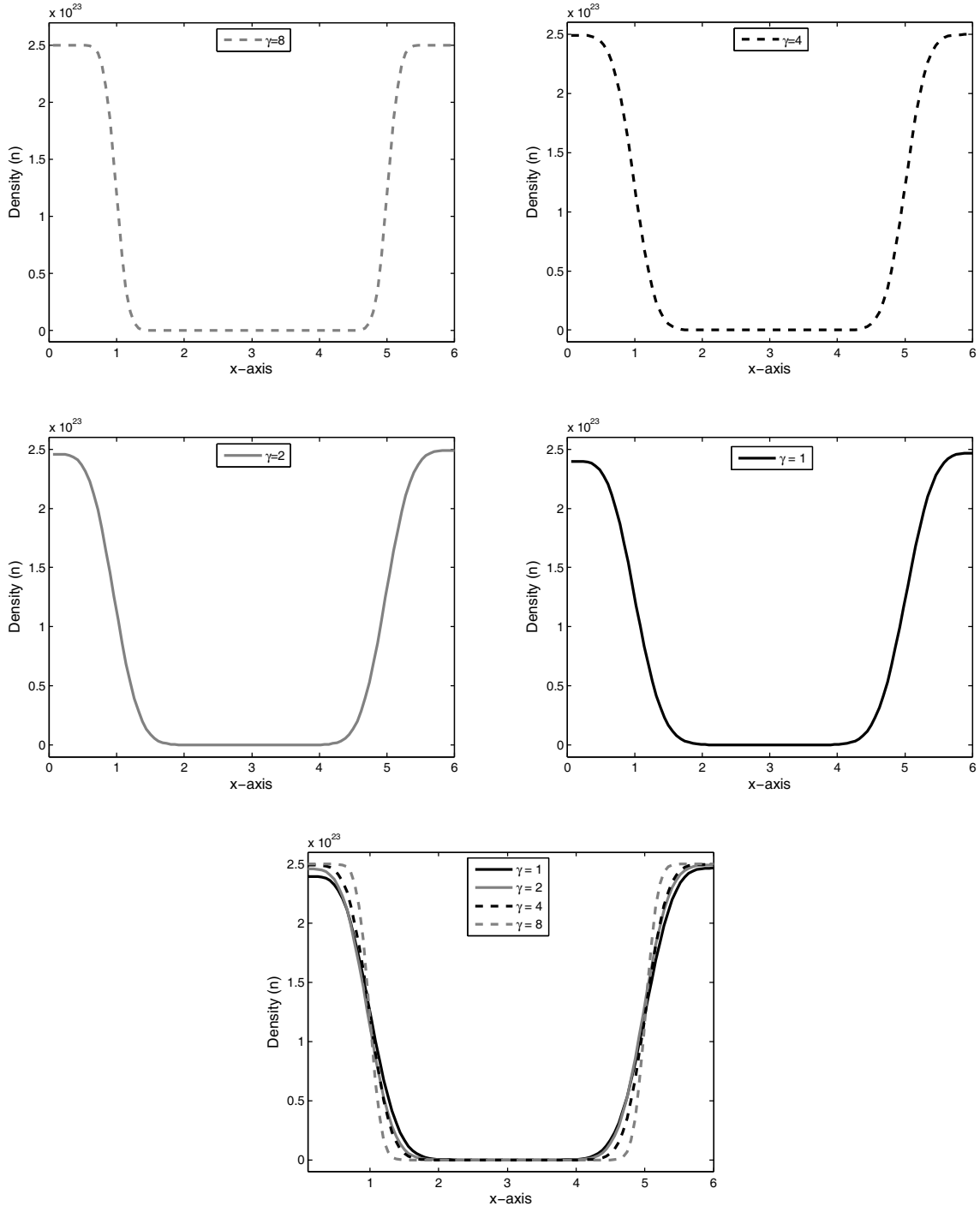

Figure 6: Effects of viscosities on density using KFVS method.

Preprints (www.preprints.org) | NOT PEER-REVIEWED | Posted: 28 May 2018 doi:10.20944/preprints201805.0381.v1

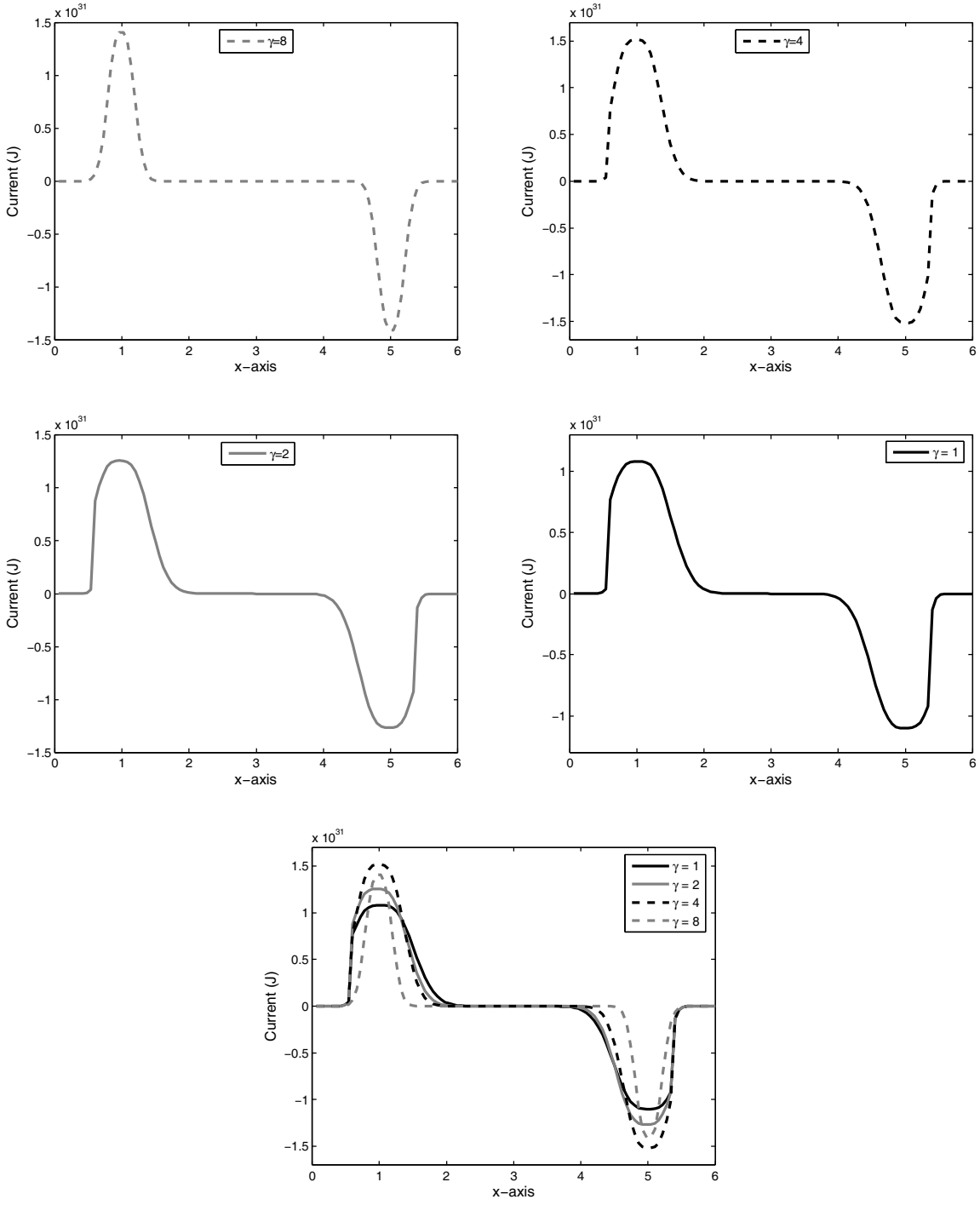

Figure 7: Effects of viscosities on current using KFVS method.